Tectonophysics 488 (2010) 150–161

Contents lists available at ScienceDirect

Tectonophysics

journal homepage: www.elsevier.com/locate/tecto

The northwestern margin of the Basin and Range province
Part 2: Structural setting of a developing basin from seismic and potential field data

Anne E. Egger [a,*], Jonathan M.G. Glen [b], David A. Ponce [b]

[a] Department of Geological and Environmental Sciences, Stanford University, Stanford, CA 94305-2115, United States
[b] U.S. Geological Survey, 345 Middlefield Road, Menlo Park CA 94025, United States

ARTICLE INFO

Article history:
Received 2 June 2008
Received in revised form 10 February 2009
Accepted 28 May 2009
Available online 6 June 2009

Keywords:
Normal fault
Northwestern Basin and Range
Gravity
Magnetics
Surprise Valley
Extensional geothermal system

ABSTRACT

Surprise Valley in northeastern California offers an ideal opportunity to examine the structural setting of a developing extensional basin due to its late Miocene to recent activity in isolation from other major normal fault-bound basins. Seismic velocity and potential field modeling help determine the nature of basin fill and identify intra-basin faults. Based on a detailed gravity and magnetic profile, we identify shallow subsurface basalt flows and several faults within the valley that may accommodate hundreds of meters of vertical offset, possibly cutting and offsetting the ~30° east-dipping Surprise Valley fault that rotated during footwall tilting of the adjacent Warner Mountains. Some of these intra-basin faults correspond with mapped Quaternary fault scarps, but others have no surface expression. These faults may represent the currently active fault system within the basin. If so, they would indicate that basin development is transitioning away from the main range-front normal fault to a new set of steep intra-basin faults that are more favorable for accommodating regional transtensional strain.

© 2009 Elsevier B.V. All rights reserved.

1. Introduction

Along the northwestern margin of the Basin and Range province, normal faulting is encroaching on the largely unextended Modoc Plateau (Fig. 1). The Surprise Valley fault (SVF) is the westernmost large-offset normal fault in the northwestern Basin and Range, and it is isolated from other large-offset faults to the east by the ~90-km wide Sheldon Plateau (Fig. 1). The SVF may have been active as early as 12 Ma (Colgan et al., 2008b), and the presence of Quaternary fault scarps and an active geothermal system suggest that it is still active today. Thus, the Surprise Valley fault and associated structures provide an excellent opportunity to study the evolution of continental extension and normal faulting.

Like many faults in the Basin and Range province that are considered active, however, the SVF has not experienced historical seismicity. Detailed geodetic data can provide some constraints on fault motion in seismically inactive regions (e.g. Friedrich et al., 2004), but the data available for the Surprise Valley are widely spaced (Hammond and Thatcher, 2005). Such data have also proven misleading in other parts of the Basin and Range when compared with geological measures of extension (e.g. Oskin et al., 2008). Paleoseismic trenching has discerned earthquake recurrence intervals along nearby Basin and Range normal faults such as the Southern Steens fault zone in northern Nevada (Personius et al., 2007b), allowing calculation of a slip rate, but similar trenching along the Santa Rosa Range fault zone yielded ambiguous results due in part to the presence of multiple fault strands (Personius and Mahan, 2005). Recent activity and slip histories can also be inferred from calculations of diffusion erosion rates of degraded fault scarps (e.g. Lee et al., 2001), but in Surprise Valley, some recent fault scarps may be buried under lake sediments or heavily modified by wave action of the long-lived pluvial lake (Reheis, 1999). Given these constraints, geophysical mapping and modeling of seismic, gravity, and magnetic data lend critical insight into the nature of structures at depth, revealing structures that do not have surface expression, and may also help resolve likely fault interactions, constraining the nature of faults and their sense of slip. These techniques have proved useful in illuminating subsurface structures and rock units in other valleys of the Basin and Range, including the Crater flat region (Brocher et al., 1998) and Dixie Valley (Blackwell et al., 2002).

The comparison with Dixie Valley is particularly apt given the presence of a geothermal system: in Surprise Valley, subsurface structures appear to play a particularly important role in the location of hot springs. In the present study, seismic velocity and potential field modeling are used to resolve the subsurface geometry of major basin-bounding faults, to identify and describe the nature of intra-basin faults, and ultimately to compare different scenarios of basin evolution. Our geophysical modeling, combined with geologic mapping, seismic reflection data, and potential field mapping suggest that the Surprise Valley fault may currently be in transition from a single,

* Corresponding author. Fax: +1 650 725 0979.
E-mail address: annegger@stanford.edu (A.E. Egger).

0040-1951/$ – see front matter © 2009 Elsevier B.V. All rights reserved.
doi:10.1016/j.tecto.2009.05.029

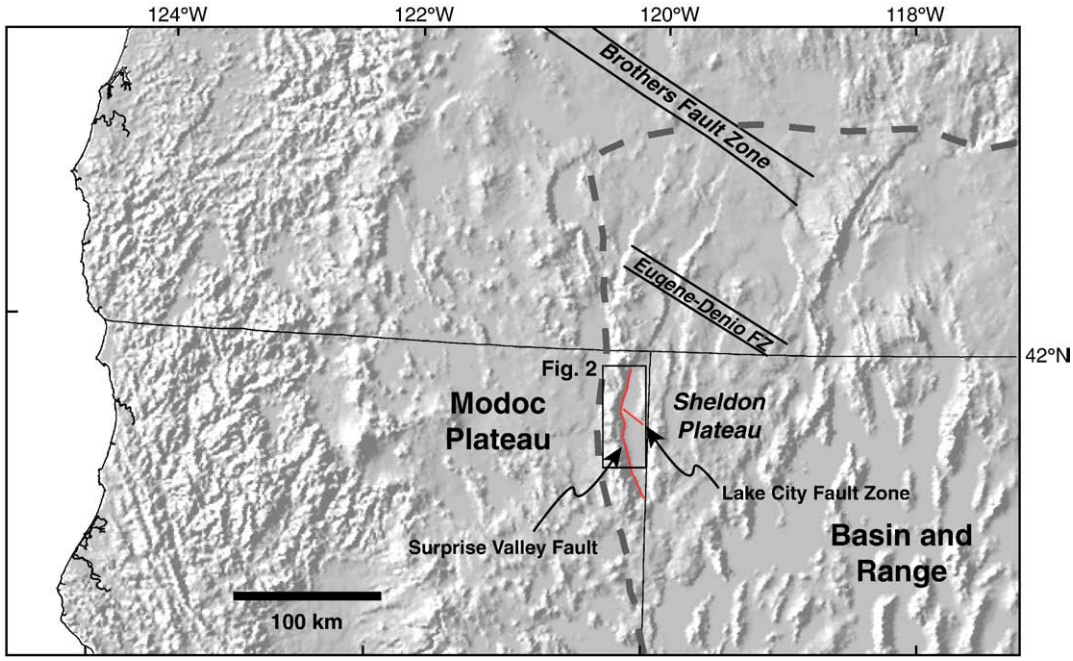

Fig. 1. Shaded relief map of the northwestern margin of the Basin and Range province. Major NW–SE-trending fracture zones are labeled. Inset box shows the study area of the Warner Range and Surprise Valley lying between the Sheldon and Modoc Plateaus, which have experienced very little extension.

large-offset normal fault to a more intra-basinal system consisting of an array of smaller-offset normal faults.

2. Geologic setting

Surprise Valley straddles the California–Nevada border, stretching about 100 km south from the Oregon border (Fig. 1). The Surprise Valley fault (SVF) separates the valley from the Warner Range to the west, which exposes a thick series of Eocene to late Miocene sedimentary and volcanic rocks (Fig. 2) (Duffield and McKee, 1986; Fosdick et al., 2005; Colgan et al., 2008a). These rock units display significant variability in thickness along strike (e.g. Egger et al., 2009). For example, the Oligocene Lake City basalt (Tlb in Fig. 2) pinches out completely from an exposed thickness of >1 km over a distance of approximately 10 km. Near the study area, these rocks have been tilted approximately 20° westward by motion along the SVF (Fig. 2). On the eastern side of the valley, low-lying ridges of 4–8 Ma basalts (Carmichael et al., 2006) dip more gently (10–15°) westward into the basin. These younger basalts are not present at the crest of the Warner Range. The lateral discontinuity of units in this region make determination of fault offset difficult, but estimates range from 3.6 km of vertical offset (Duffield and McKee, 1986) to as much as 8 km (Fosdick et al., 2005).

Like many normal faults, the SVF has a corrugated, curvilinear trace and the range front makes several abrupt steps along its length (Fig. 2). A particularly prominent step occurs at the boundary between the Cedarville and Lake City segments where the SVF changes strike abruptly by ~45° and the number of Quaternary fault scarps increases (Fig. 2). This region resembles a segment boundary (as defined by Zhang et al., 1999) or accommodation zone (e.g., Faulds and Varga, 1998), as it coincides with an abrupt widening of the valley to the south, a large number of small-offset faults that cut the young basalts (Fig. 2), and a topographic high separating the upper and middle playa lakes in the valley, remnants of a Pleistocene pluvial lake that reached a depth of ~500′ (Reheis, 1999). Within the topographic high, a wide zone of faults and fractures that has been previously mapped by Hedel (1984) as the Lake City Fault Zone (LCFZ) cuts northwestward across the valley (Fig. 2). The nature and origin of the LCFZ are enigmatic, though geophysical studies suggest that it accommodates little vertical offset (Griscom and Conradi, 1976; Hedel, 1984; Glen et al., 2008). Regionally, the LCFZ shares a NW–SE trend with Fandango Valley (Fig. 2) and the Brothers and Eugene-Denio Fault Zones in Oregon (Fig. 1), both of which have been shown to accommodate oblique right-lateral slip (Lawrence, 1976; Crider, 2001).

The LCFZ is closely associated with the Surprise Valley geothermal system, the object of periodic exploration since the spectacular mud-volcano eruption near the Lake City hot springs in 1951 (LC in Fig. 2) (White, 1955). While this association of structures and geothermal activity has long been recognized (Hedel, 1981; Benoit et al., 2004), the details of the interactions between the LCFZ, the Surprise Valley fault, and other N–S-trending structures have proven difficult to incorporate into a geothermal and hydrological model. In fact, the majority of springs in Surprise Valley do not occur along either the LCFZ or the SVF, and instead are offset basinward from faults on both the east and west margins of the valley (Fig. 2). Some springs occur along mapped Quaternary fault scarps, but many do not — particularly the geothermal springs (Fig. 2). Renewed exploration, including drilling near Lake City in 2005 conducted by Amp Resources (Benoit et al., 2005; Miller et al., 2005), a magneto-telluric survey of the same region by Enel-North America (Andrew Rael, pers. comm., 2008), and investigation into He-isotopes in spring waters (Barker et al., 2005) have all sought to better characterize this geothermal system and its relation to surface and subsurface structures. Measured $^{3}He/^{4}He$ ratios also provide insight into the basin-scale interactions between structures. In general, higher values represent a larger mantle component to the fluids, while lower values represent greater crustal contribution and/or residence time in the crust (Kennedy and van Soest, 2006). The ratios measured in geothermal waters near Fort Bidwell are markedly higher than those seen in springs that fall along the LCFZ (Barker et al., 2005), suggesting that the LCFZ may provide lateral permeability that does not occur along the range-front fault, allowing waters to circulate and mix in the crust for longer periods of time.

A seismic reflection profile was collected across the valley in 2004 (Fig. 2) (Lerch et al., 2008). In the reflection profile, the most prominent reflector is a gently-dipping feature on the western side of the valley, presumed to be the Surprise Valley fault (see Lerch et al., 2010-this issue). When corrected for apparent dip related to crossing

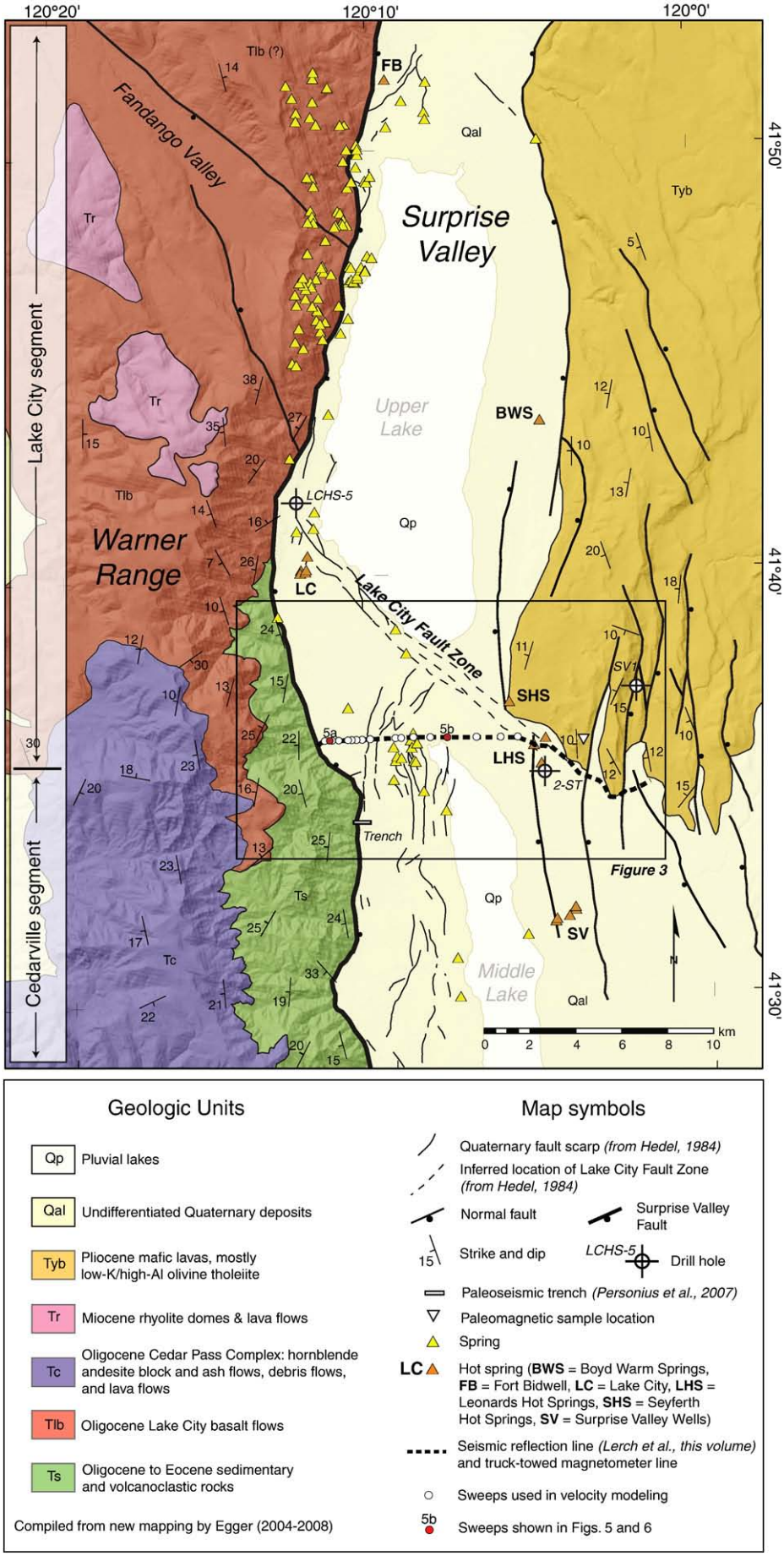
120°20'
120°10'
120°0'
41°50'
41°40'
41°30'
Lake City segment
Cedarville segment
Fandango Valley
Surprise Valley
Warner Range
Upper Lake
Middle Lake
Lake City Fault Zone
Figure 3
Trench
FB
BWS
LC
SHS
LHS
SV
LCHS-5
2-ST
SV1
5a
5b
Qal
Qp
Tyb
Tr
Tlb
Tlb (?)
Ts
Tc
km
0 2 4 6 8 10
Geologic Units
Qp Pluvial lakes
Qal Undifferentiated Quaternary deposits
Tyb Pliocene mafic lavas, mostly low-K/high-Al olivine tholeiite
Tr Miocene rhyolite domes & lava flows
Tc Oligocene Cedar Pass Complex: hornblende andesite block and ash flows, debris flows, and lava flows
Tlb Oligocene Lake City basalt flows
Ts Oligocene to Eocene sedimentary and volcanoclastic rocks
Compiled from new mapping by Egger (2004-2008)
Map symbols
Quaternary fault scarp (from Hedel, 1984)
Inferred location of Lake City Fault Zone (from Hedel, 1984)
Normal fault
Surprise Valley Fault
Strike and dip
Drill hole
Paleoseismic trench (Personius et al., 2007)
Paleomagnetic sample location
Spring
Hot spring (BWS = Boyd Warm Springs, FB = Fort Bidwell, LC = Lake City, LHS = Leonards Hot Springs, SHS = Seyferth Hot Springs, SV = Surprise Valley Wells)
Seismic reflection line (Lerch et al., this volume) and truck-towed magnetometer line
Sweeps used in velocity modeling
Sweeps shown in Figs. 5 and 6

the fault at an oblique angle, this reflector indicates a fault dipping approximately 30° to the east — a relatively shallow dip for an active range-bounding normal fault. In contrast, a paleoseismic trench located 3.8 km south of the seismic reflection profile (Fig. 2) revealed a normal fault dipping 68° to the east, cutting and offsetting fine-grained lake sediments (Personius et al., 2007a). No single unit could be tied across the fault, but an ash that correlates with the 7630-year-old ash from the Mt. Mazama eruption in the Oregon Cascades was exposed in the hangingwall, providing a minimum offset and displacement of ~1 mm/year. It is possible that the 68° fault observed in the trench is a listric splay of the Cedarville segment of the SVF, which shallows to ~30° at depth (e.g. Axen et al., 1999). Another possible interpretation is that the steeper fault exposed in the trench cuts the gently-dipping fault imaged in the seismic profile. These two possible interpretations lead to different conclusions about both the geothermal system and the seismic hazard potential for the valley. The geophysical methods applied here may help distinguish between these two interpretations where detailed surface mapping cannot.

3. Data collection methods

We used a combination of seismic velocity and potential field modeling to better constrain the present geometry of the range-bounding fault system and to define the offsets and significance of the faults mapped within Surprise Valley. Seismic velocity modeling can constrain the depth of a basin and identify abrupt changes in velocity that create reflections indicative of lithologic contacts. Variations in gravity and magnetics occur due to lateral contrasts in rock density and magnetic properties (induced and remanent magnetizations), respectively. The shape, depth, and rock properties associated with a source all determine the character of its potential field anomaly. As a result, the combination of seismic and potential field data can be used to resolve the geometry of known or concealed features, particularly when combined with other geologic constraints provided by the regional tectonic setting and surface geologic mapping. A series of detailed transects of ground-based magnetometer data and closely-spaced gravity data was collected (Glen et al., 2008) and digitized (from Griscom and Conradi, 1976) in order to perform joint gravity and magnetic modeling and interpretation. One of these transects was along the high-resolution seismic reflection line described by Lerch et al. (2010-this issue) (Figs. 2 and 3). These detailed transects were combined with regional gravity and magnetic field data (Ponce et al., in review).

3.1. Gravity data

Gravity data were compiled from a variety of sources (Griscom and Conradi, 1976; Plouff, 1977; Snyder et al., 1981; Ponce, 1997; Tilden et al., 2005; PACES gravity data at http://paces.geo.utep.edu/, 2008; Ponce et al., in review). In addition, we collected 793 new gravity stations to provide roughly 1 km regional station-spacing in the valley, 1–2 km spacing in the ranges, and 100–500 m spacing along several detailed transects that cross the valley (Fig. 3b). All gravity data collected for this study were tied to a primary base station in Alturas, California (Jablonski, 1974).

New data were reduced using standard gravity methods that include: earth-tide, instrument drift, latitude, free-air, simple Bouguer, curvature, terrain, and isostatic corrections (Blakely, 1995) to yield isostatic anomalies. Regional data were corrected from observed gravity values to the same datum and using the same reduction parameters as our new data. The gravity map and profile derived from these data (Figs. 3a and 4) reflect anomalies produced by lateral variations in crustal density. Maximum horizontal gradients (MHGs) in gravity were calculated, following the technique of Blakely (1995), to aid in identification of these contrasts (Fig. 3a). Because MHGs tend to lie over near-vertical boundaries representing prominent rock-property contrasts, they are useful in estimating the extent of rock units and locating faults with vertical offset.

3.2. Magnetic data

Sources of magnetic data employed in this study include a high-resolution aeromagnetic survey of the LCFZ-area and a truck-towed magnetometer profile (USGS, 1981; Kucks et al., 2006; Ponce et al., in review). The high-resolution survey (see Fig. 3b for area covered) was flown at an elevation of 122 m above ground with flight lines oriented north–northeast and spaced 1/4 mile apart (survey 81-997; USGS, 1981). Data from this survey were derived from digitized contours of the original survey maps. Ground-magnetic measurements were collected using a truck-towed cesium-vapor magnetometer across the valley (Fig. 3). A centrally located portable proton-precession base-station magnetometer was used to record diurnal variations of the Earth's magnetic field during the survey. The data were corrected for the diurnal variations, and filtered to remove cultural noise such as passing cars, culverts, fences, and power lines. The map and profile derived from these data (Figs. 3b and 4) therefore reflect variations in the magnetic field that arise largely from contrasts in rock magnetic properties attributable to a number of different causes including depths to the magnetic sources, crustal structures juxtaposing different rock types, metamorphism and alteration, variations in remanent magnetization, and variations in the concentration and type of magnetic minerals within rock units.

4. Features of potential field data

The focus of this work is on features identified in profiles along the model transect (Fig. 4), but regional and high-resolution gravity and magnetic maps were useful in identifying the lateral extent and character of anomalies away from the transect, an important component of interpreting the nature of sources from which anomalies arise, and critical to modeling features off-axis to the transect. The most prominent features in the gravity map (Fig. 3a) include a broad gravity low occupying the valley, reflecting low-density alluvial and volcanic basin-fill deposits, and a broad gravity high over exposed or inferred mafic volcanic units in the Warner Mountains and along the western margin of the valley floor. Situated between these two features is a moderate-to-steep gravity gradient that occurs along the Surprise Valley fault. The most prominent feature in the magnetic field map is a low that occurs within the central part of the valley (Fig. 3b). Magnetic highs flanking this low along the margins of the basin (a, b, and c in Fig. 3b) do not correspond with surficial features, and thus are inferred to represent the presence of highly magnetic mafic rocks in the underlying volcanic basement and thin basalt flows interbedded with the basin sediments. Smaller magnetic lows may represent mafic igneous units that are reversely magnetized or rocks that have undergone hydrothermal alteration that has destroyed or alter magnetic minerals (thin dashed line in Fig. 3b).

The prominent gravity and magnetic highs on the west side of the valley are also, not surprisingly, the most conspicuous features along the model transect (Fig. 4). These appear as broad, eastward-

Fig. 2. Simplified geologic map of the northern Warner Range and Surprise Valley, draped over a shaded relief map. See legend for description of units and symbols. Location of seismic line and Vibroseis sweeps selected for velocity modeling shown.

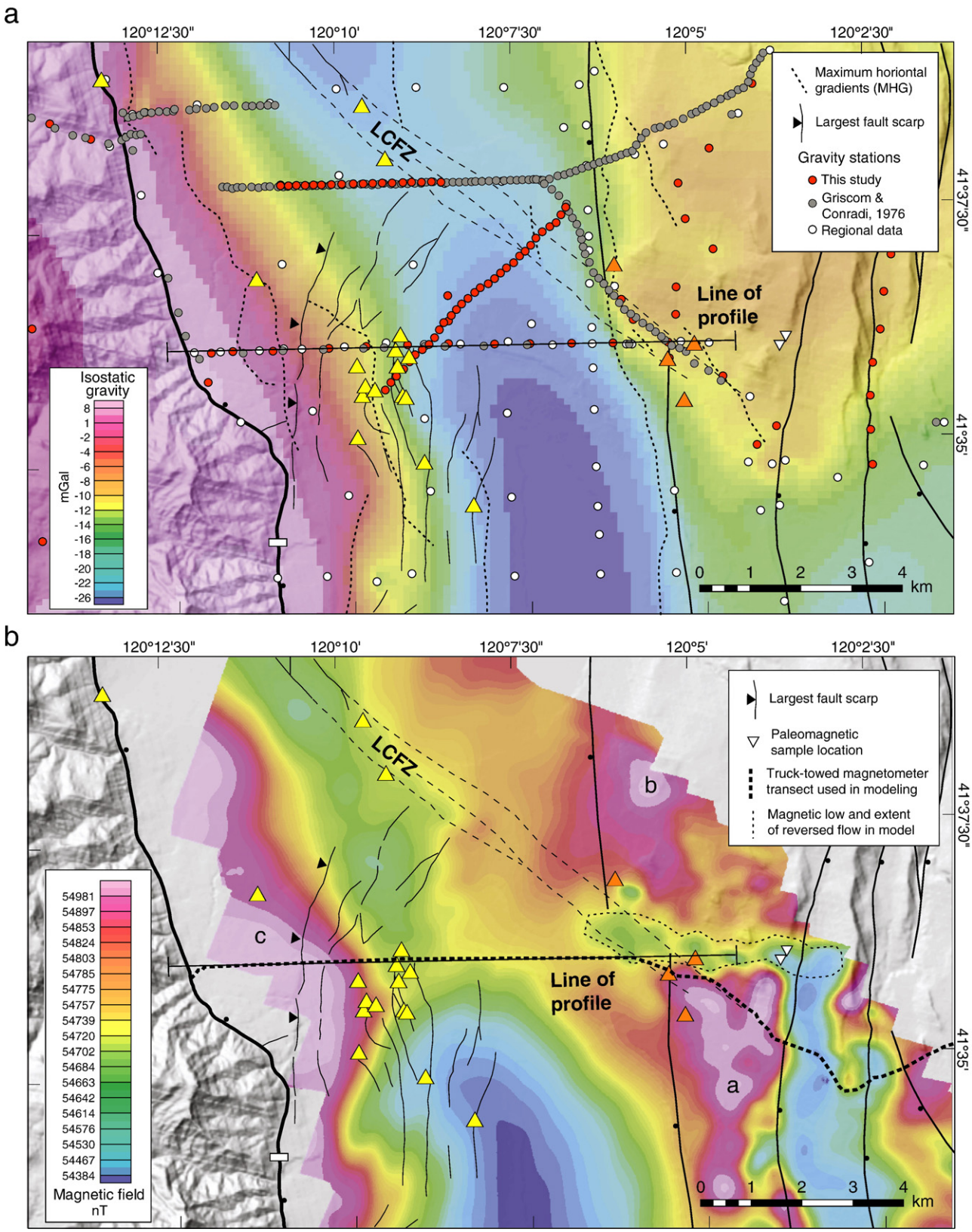

Fig. 3. a. Isostatic gravity map of study area including all gravity stations used to derive the grid. Symbols used here are the same as in Fig. 2; refer to Fig. 2 legend for complete description. b. High-resolution aeromagnetic map of study area (from U.S. Geological Survey OF 81-997-4077). Note the numerous features with high magnetic susceptibility (bright pink areas) but no surface expression in the topography. Symbols used here are the same as in Fig. 2; refer to Fig. 2 legend for complete description.

decreasing ramps, largely coincident with each other, that drop from highs in the west to lows in the central portion of the valley. The gravity profile drops over 6 km to the lowest values observed along the profile, marking what is interpreted to be the deepest part of the basin (Fig. 4). The amplitude and frequency content of this feature suggest that it is caused in large degree by rocks at depth, typical of the

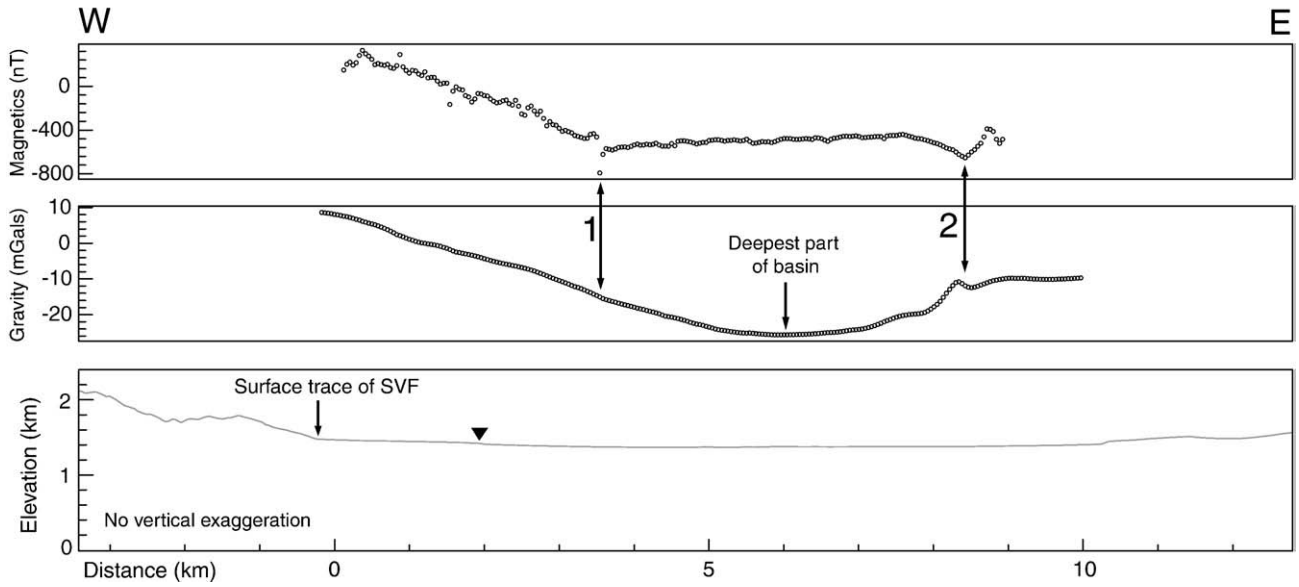

Fig. 4. Potential field data and topographic profile used in the model. Line of profile is shown in Fig. 3. Gravity profile is extracted from gridded, detailed data; magnetic data are from a truck-towed magnetometer transect. Both are limited to the extent of detailed data along a straight-line transect. Black triangle indicates location of topographically most significant Quaternary fault scarp.

gradients seen at other large-offset normal faults in the Basin and Range (e.g. Pakiser and Kane, 1965; Okaya and Thompson, 1985). Not even the most prominent fault scarp (Fig. 4, black triangle) is represented by any significant change in the gravity profile. In contrast, a series of small amplitude, high-frequency magnetic anomalies, superimposed on the magnetic ramp, does suggest the presence of some shallow magnetic sources. The most prominent of these occurs at the eastern terminus of the ramp where the field gradient changes abruptly (Fig. 4, feature 1). This feature lies within the basin, east of the surface trace of the SVF, and, corresponds with a zone of fault scarps and springs (Fig. 2).

A second feature of interest is a coincident minor gravity high and magnetic low at 8.5 km (Fig. 4, feature 2). This feature is proximal to several major hot springs on the east side of the valley as well as the inferred southeastern extension of the Lake City Fault Zone (Fig. 3a and b). The low in the magnetic profile is part of a narrow, elongate E–W-trending magnetic low that can be seen in map view (Fig. 3b). At the eastern extent of this low, basalt flows are exposed at the surface. Results from our preliminary paleomagnetic study of samples taken from these flows in the vicinity of the magnetic low indicate that they are reversely magnetized — a fact that appears to account for the low in the potential field model (see discussion below). The corresponding minor gravity high is associated with a series of MHGs in the gravity data (Fig. 3a) that trends N–S, nearly perpendicular to the negative magnetic anomaly and roughly parallel with the range front.

These two features proved most challenging to replicate with potential field modeling based solely on mapped geology and reflection seismic data. Thus, we began with a seismic velocity model to help constrain the geometry of the potential field model.

5. Modeling

5.1. Seismic velocity modeling

The 16-km high-resolution seismic reflection/refraction profile modeled in this study was collected in September 2004 with the Network for Earthquake Engineering Simulation (NEES) tri-axial (T-Rex) vibrator. The details of this survey technique are given in Lerch et al. (2008) and the results are described by Lerch et al. (2010-this issue). Data processing for velocity modeling consisted of standard techniques: picking first arrivals in selected sweeps, forward modeling, and inversion. Fifteen sweeps located within the western 9 km of the line were selected based on roughly even spacing and data quality (Fig. 2). A sweep from the western end of the line shows fast first arrivals (low slope of first arrivals on consecutive traces) within 2 km east of the sweep (Fig. 5a). In contrast, a sweep closer to the center of the basin (Fig. 5b) shows much slower first arrivals (steeper slope in arrivals on consecutive traces). The first reflection hyperbola appears at approximately 600 ms, likely reflecting off a dense basalt flow within the lake sediments visible in the reflection profile (see Fig. 2 in Lerch et al., 2010-this issue). Both east and west of source point 13971, the first arrivals flatten out, most noticeably to the west, showing the presence of higher seismic velocities at depth.

We used RayGUI 2.3 for our forward and inverse modeling, a GUI by Song and ten Brink based on Colin Zelt's RayInvr code (Song and ten Brink, 2004; Zelt and Smith, 1992). The velocity model is constrained by 1580 picks with an uncertainty of <100 ms on all picks except those from the westernmost six receivers, for which we accepted a larger uncertainty of 200 ms during modeling to accommodate their location up to 500 m south of the profile and west of the Surprise Valley fault. Given constraints from geological mapping, published Quaternary fault scarps (Hedel, 1984), and seismic reflection data (Lerch et al., 2010-this issue), we used forward modeling to achieve a working model consisting of three phases of arrivals that correspond to three discontinuous layers within the valley reaching a depth of approximately 1.5 km (Fig. 6). Iterative inversion produced only minor velocity changes and little improvement in travel time residuals (T_{RMS}), shown in Table 1. The uppermost layer (phase 1 in Table 1) is best defined with 948 picks and a T_{RMS} of 0.033 s; phases 2 and 3 are based on far fewer picks and have greater travel time residuals associated with them.

The velocity model is shown in Fig. 6 overlain on the seismic reflection profile (see Lerch et al., 2010-this issue for more detail on the reflection profile), along with the modeled arrivals for the two sweeps shown in Fig. 5. A notable feature of the model is the marked asymmetry across the basin, both in velocities and in the dips of modeled units. This suggests a westward dip to the main part of the basin and faster velocities on the west. Although it was developed independently of the reflection profile, the velocity model has several

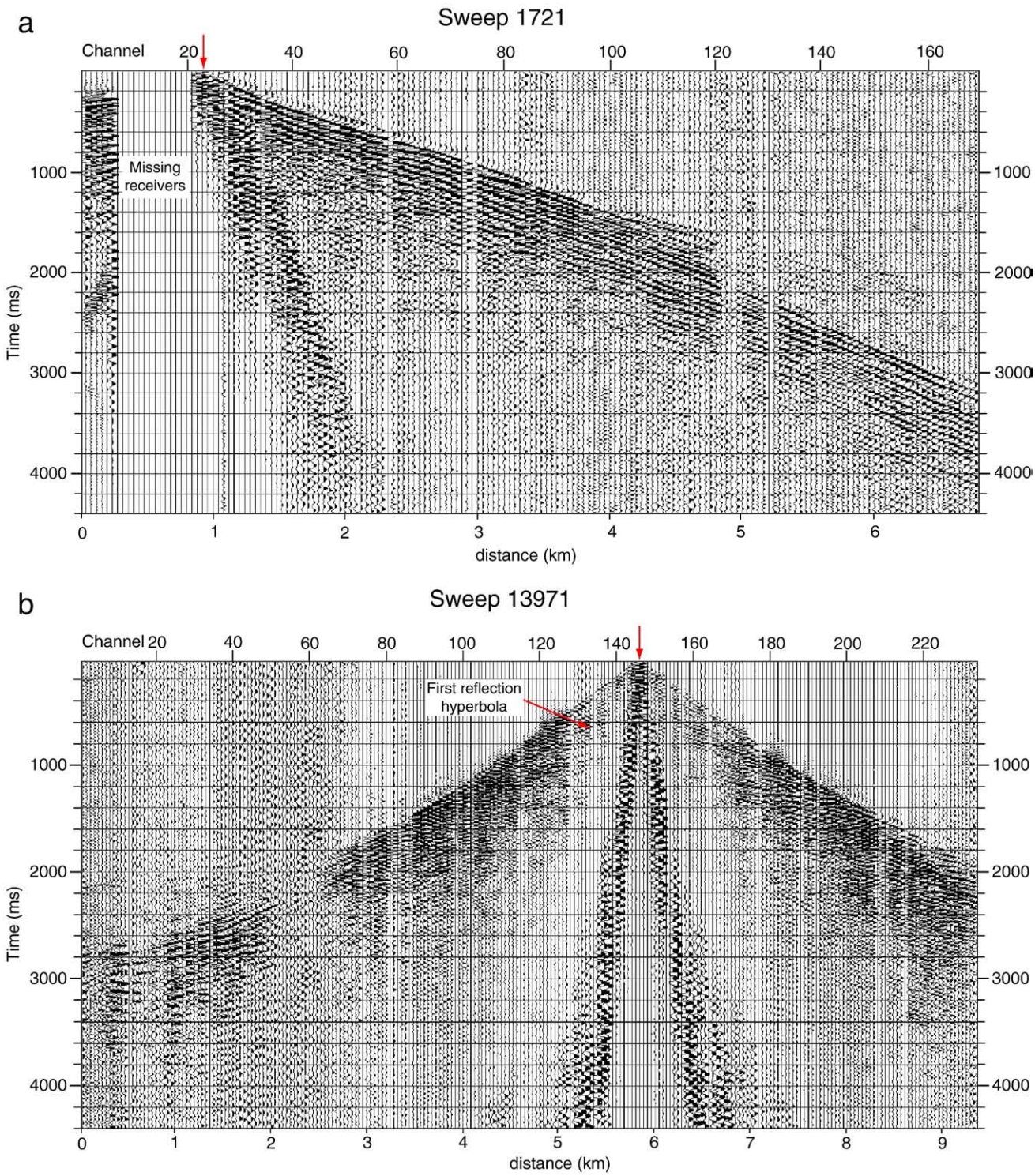

Fig. 5. a. Sweep 01721 from west end of line; location of Vibroseis truck marked by red arrow here and in Fig. 6 and by a red circle in Fig. 2. b. Sweep 13971 from central portion of the basin; location of Vibroseis truck marked by red arrow here and in Fig. 6 and by a red circle in Fig. 2.

features that match aspects of the reflection section. The moderately dipping feature at the base of the model matches well with the reflector assumed to be the Surprise Valley fault; this feature cannot be directly constrained in the model given the limit of reversed ray coverage (shown by the thick dashed line in Fig. 6b), but was introduced to provide a suitable gradient to create turning rays. In addition, the transparent region labeled "zone e" and interpreted as fan deposits by Lerch et al. (2010-this issue) corresponds to higher velocities than those seen in the main depocenter. The dashed unit in the model with a velocity gradient of 2.0–2.5 km/s created some problems: although it improved the travel time residuals for sweeps coming from the west, it decreased the fit for sweeps coming from the east. We included it in the final model, however, because it matches well with a zone with prominent reflectors in the reflection profile. The modeled geometry of this feature suggests that it may be bounded to the east by a steeply-dipping normal fault.

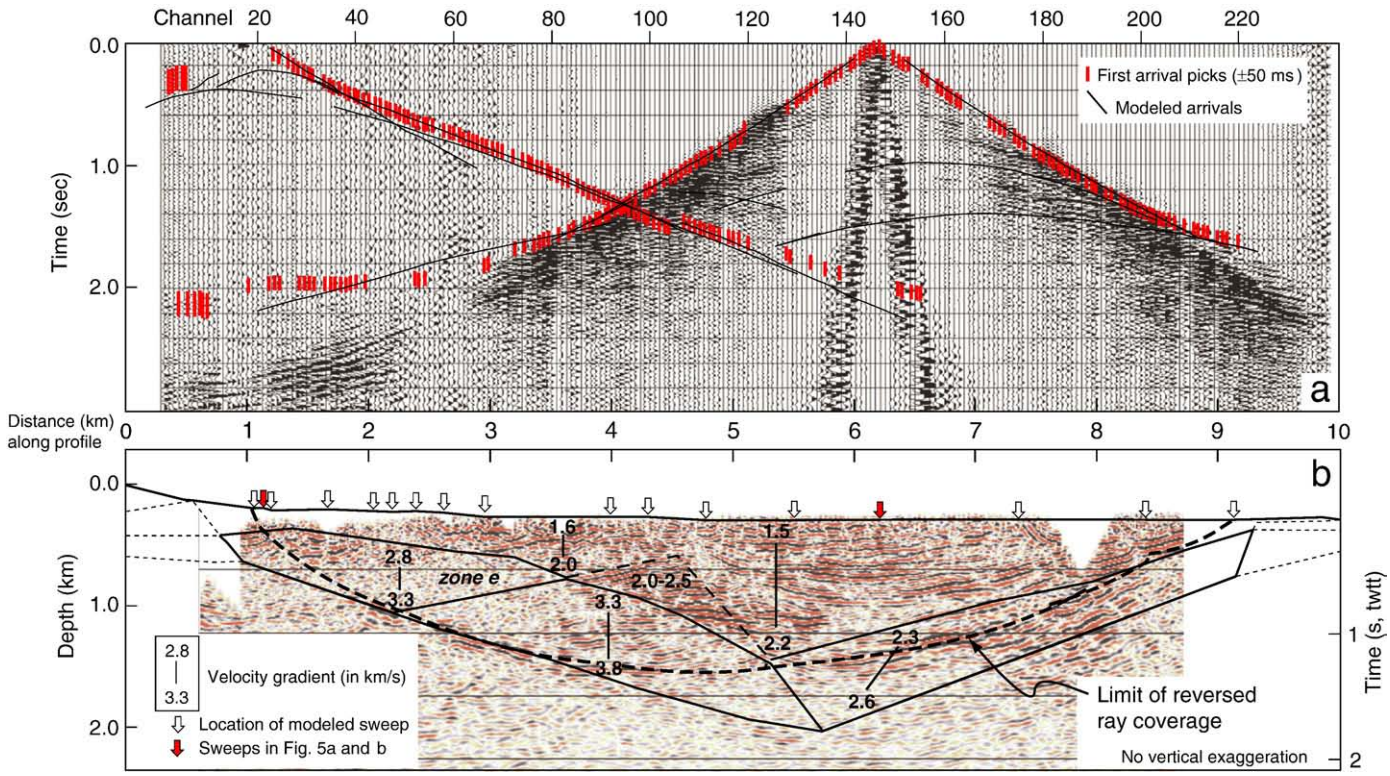

Fig. 6. (a) Observed first arrivals (red lines) with 100 ms errors and modeled results (black lines) from the two example sweeps shown in Fig. 5a and b. (b) Velocity model (see Table 1 for number of picks used and travel time residuals) overlain on a seismic reflection profile. Depth on left axis, two-way travel time (ttwt) on right axis. Wide dashed line shows the deepest limit of ray coverage. The highest velocities at the base of the basin were introduced into the model to provide suitable gradients to create turning rays, but are not directly observed from the data. "Zone e" is the relatively transparent zone in the reflection profile noted and described in Lerch et al. (2010-this issue). See text for further explanation of features.

This velocity model, along with the constraints provided by surface geology and seismic reflection data, was used as a starting point for potential field modeling.

5.2. Two-dimensional potential field modeling

Using the seismic velocity model as a starting point to constrain basin structures and densities, we developed a two-dimensional (2D) potential field model using a 2D forward modeling package (GMSYS®) (Figs. 7 and 3 for location). The focus of our modeling efforts was a 9-km profile for which we had detailed gravity and magnetic data. In addition to modeled velocities for units in the basin, the model incorporates information from our mapping, wells and drill-cores (Fig. 2; Benoit et al., 2005), seismic reflection (Lerch et al., 2010-this issue), and measured rock-property data (Ponce et al., in review). Rock units consist of horizontal tabular prisms or blocks aligned with their longest axes perpendicular to the profile. Their surface extents are consistent in size, shape, and orientation with exposed rock units and with features observed in the seismic reflection profile (Lerch et al., 2010-this issue) and velocity modeling. Although the profile is roughly perpendicular to the strike of the primary basin-bounding faults, it crosses the range-front fault near a significant left step, creating an asymmetry in the crust to the north and south of the profile. We initially attempted to model the effects of this asymmetry but found its influence to be minimal and thus did not incorporate it into the final model.

To begin, we determined P-wave velocity-derived densities for subsurface units in the basin using the Brocher (2008) modification of the Nafe–Drake relationship (Ludwig et al., 1970) that provides a best-average velocity-to-density conversion based on a broad range of common rock types, including a simple density–depth function to account for compaction. For exposed units, we used magnetic susceptibility and density values measured on hand samples collected in the field area (Ponce et al., in review). Induced components of magnetization were calculated assuming an ambient field of 51,850 nT with an inclination of 65° and declination of 15°. Remanent magnetization directions of the model source bodies were assumed to be parallel to a time-averaged geocentric axial dipole field direction with an inclination of 65°, and declination of 0° (or declination of 180°, inclination of −65°, in the case of one reversely magnetized unit). Magnetizations were assumed for units based on values consistent with published values for appropriate rock types. Well logs from two exploratory geothermal wells beyond the extent of the velocity model (Fig. 2) were used to estimate sediment depths.

Rock-property values assigned to unexposed shallow-to-mid-upper crustal units (particularly on the west side of the valley) are poorly constrained. The only information on crustal lithology at these levels comes from the core LCSH-5 where mafic volcanic units occur near the base of the drill-core at a depth of 4200′ (Fig. 2) (Miller et al., 2005). Extrapolating these units to the lower part of the model appears to be reasonable, since relatively high densities and magnetic

Table 1
Errors associated with seismic velocity model shown in Fig. 6.

Phase	Points used	T_{RMS} (s)	Chi^2
All	1247/1580	0.052	0.26
1	948	0.033	0.112
2	199	0.096	0.92
3	100	0.068	0.358

The phase refers to the number of layers that modeled rays pass through. "Points used" refers to the number of picked first arrivals used in the model. T_{RMS} is the square root of the sum of the square of the travel time residuals (in seconds), a measure of the difference between the observed and modeled travel times. Normalized chi-square values in the final column are an indication of goodness of fit.

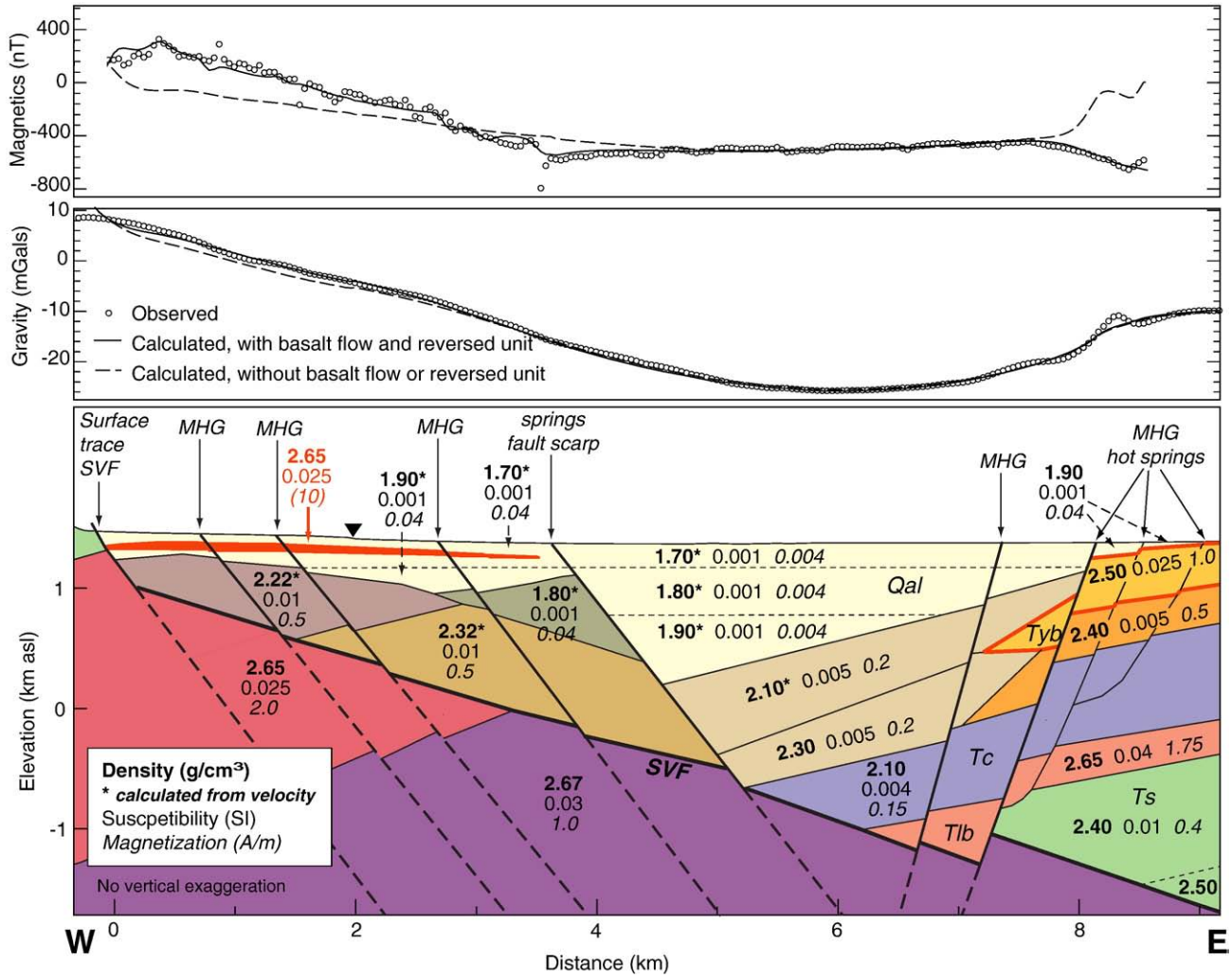

Fig. 7. Potential field model. Units labeled Qal, Tyb, Ts, Tc, and Tlb correspond to geologic units shown in Fig. 2. Properties of other units are inferred based on seismic velocity modeling and achieving the best-fit potential field model as described in the text. Inferred steeply-dipping faults are shown in solid lines through the basin and dashed into the basement to indicate that modeling cannot determine if these faults sole into the Surprise Valley fault (SVF on figuere) or cut it at depth as we show here. Annotation on these faults indicates correlations with features shown in Fig. 3. Black triangle indicates location of topographically most significant Quaternary fault scarp. Features in red are not included in the dashed line model calculations; they are included in the solid line calculations.

susceptibilities, consistent with the basal-core samples, are required to match the observed gravity and magnetic profiles. Because metamorphic or crystalline basement rocks are not exposed anywhere in the study area, nor were they penetrated in the core or any drill holes, densities for crust comprising the deepest parts of the model are also poorly constrained so we use average values for continental crust.

6. Model features

Initial development of the model based on the seismic reflection section and velocity modeling within the valley (described above) produced a reasonably good fit with the observed gravity profile, particularly on the west side of the basin. Several modifications, however, were required to achieve a best-fit model (Fig. 7) that also accounted for features observed in the magnetic profile. These modifications consist of (1) making significant lateral changes in the thickness of units in the subsurface, (2) adding several faults with vertical offset which are not expressed on the surface, (3) assigning a reverse magnetization and confined extent (perpendicular to the plane of the transect) to mafic flows on the east side of the valley, and (4) adding a shallow, mafic basalt flow on the western side of the basin.

The most significant changes in thickness are in the subsurface units on the eastern side of the profile. These units correspond with Oligocene volcanic rocks exposed in the Warner Range, where they are observed to vary widely in thickness (Fig. 2). The nature of the exposure in the Warner Range, the geologic interpretation of these two units as a progression from more mafic to intermediate arc volcanism (Colgan et al., 2008a), and the thick exposure of Oligocene tuff in the Hays Canyon Range immediately southwest of the study area (Carmichael et al., 2006) support this modification to the model. By increasing the thickness of tuff (Fig. 7, Tc, light purple) at the expense of basalts and andesites (Fig. 7, Tlb, light red), we were able to better fit the relatively low gravity values at the eastern end of the profile.

We also modified the initial model by adding several steeply-dipping faults with relatively minor (but measurable) vertical offsets. Some of these inferred faults correspond to both mapped Quaternary fault scarps and maximum horizontal gradients (MHGs) in the gravity data (Fig. 7), validating the correlation between MHG and structural features and suggesting that these relatively minor topographic scarps may accommodate significant offset at depth. Other inferred faults

match MHGs and gradient changes in the magnetic profile but do not correspond to surface features (Fig. 7). In map view, these MHGs form continuous, parallel lines within the basin, variably 1–3 km inboard from the range-front faults (Fig. 3a). They roughly parallel the main range-front fault but do not exhibit the same corrugation. These features may indicate a nested graben in the interior basin, similar to those observed in Dixie Valley (Smith et al., 2001) and Verdi Valley (Ramelli et al., 1999). The size of the anomalies marked by the MHG differs considerably, however, from 1–2 mGal on the west side to 3–4 mGal on the east (Fig. 7). The eastern MHG and associated anomaly are proximal to two of the major geothermal springs: Leonards Hot Spring and Seyferth Hot Spring (Fig. 2). The hydrothermal alteration associated with these springs could lead to enhancement of the positive gravity anomaly through cementation and densification of surrounding rocks.

The lack of surface expression of these inferred intra-basin faults may indicate that they are no longer active. However, the faults inferred solely from the gravity and magnetic profiles all lie well within the youngest alluvium deposits of the Pleistocene Lake Surprise, and any surface ruptures within the last 10 ka (or perhaps even much younger, given the modern presence of seasonal lakes) could have been removed through wave action and slumping. It is worth noting that, although this profile does not cross the LCFZ, elsewhere, Griscom and Conradi (1976) mapped the LCFZ on the basis of discrete change in frequency and amplitude of noise in several magnetic profiles that cross the zone, in contrast with the changes in gradient seen across faults with vertical offset.

Interestingly, there is no significant feature in either the gravity or magnetic profile that correlates with the largest topographic fault scarp within the basin, the northward projection of the Cedarville segment of the fault (indicated by the black triangles on the model in Figs. 7 and 3). Typically, a complex faulting geometry exists at depth at these segment boundaries early in the extensional history of a region (Anders and Schlische, 1994; Crider, 2001; Marchal et al., 2003), but it appears that the presence of a segment boundary is no longer a significant influence on the fault geometry in this region.

The dashed calculated model fit line in Fig. 7 includes these first two modifications, but the model still shows significant misfits. The following two modifications were made to account for these misfits; the solid calculated model fit line in Fig. 7 includes them. In order to model the magnetic low on the east end of the profile, we assigned a reverse magnetization to Tyb (outlined in red in Fig. 7) that crops out along an east-trending magnetic low observed in the high-resolution magnetic map (dotted line in Fig. 3b). This modification is based on paleomagnetic results from samples taken from near the low (white triangles, Fig. 3b) that indicate these flows are reversely magnetized. As noted above, the declination of this unit was changed to 180° and inclination to −65°. Although the lateral extent of these reversed flows is not yet known, assuming that they are confined to the region of the low (i.e., limiting their extent perpendicular to the plane of the model to the extent of the low observed in Fig. 3b) largely helps to account for the low in the potential field model.

The final modification to the model is the most significant and also the most speculative: in order to account for a significant deficiency in the calculated magnetic profile on the western end of the model, we added a thin, faulted mafic lava flow interbedded with the alluvial deposits (Fig. 7, red body in the shallow subsurface on the west side of the valley). Steps in the flow, resulting from faulting, proved an effective means of reproducing sharp gradients in both potential field profiles and in accounting for the magnitude and shape of the ramps, particularly in the magnetic profile.

The presence of flows interbedded with the alluvium is speculative because there is no surficial evidence for any flows sourced or localized along the range front on the western side of the valley. Their inclusion in the model, however, can account for the sharp changes in potential field gradients that require shallow sources, and they provide a convenient explanation for the higher-than-expected densities and susceptibilities inferred for the fan deposits. Our mapping has shown that localized flows are common in the young basalt-dominated hills to the NE of the study area (Fig. 2), and their lack of surface exposure here could reflect a short-lived episode of volcanism that has been subsequently buried by sedimentation. Regardless, it is clear that the magnetic profile is influenced by sources both at depth and in the upper few hundred meters of the profile, and a shallow basalt flow interbedded with and overlying the fan deposits can account for the high-frequency features in the magnetic profile.

7. Implications for basin development

Our model suggests two possibilities for the tectonic setting and structural development of Surprise Valley, each of which offers different implications for ongoing evolution of the basin. The first possibility is that extension is occurring along a single significant range-front fault. In this case, the multiple intra-basin faults, particularly those observed along the west side of the profile, represent listric steepening of strands of the main, active SVF imaged at a shallow angle at depth, as described by Lerch et al. (2010-this issue). This relationship between surface expressions of faults and their equivalents at depth has been demonstrated in many other places, including large systems such as the Gulf of Mexico (e.g. Bradshaw and Zoback, 1988) and Gulf of Corinth (Goldsworthy and Jackson, 2001) as well as within other portions of the Basin and Range, including Dixie Valley (Caskey et al., 1996) and the Sierra El Mayor of Baja California (Axen et al., 1999).

Another possibility is that the intra-basin faults represent the nascent and currently active fault system that is inferred to cut the SVF at depth, which may have become too shallow, given frictional resistance, to continue to slip (e.g. Proffett, 1977; Surpless et al., 2002) or may no longer be oriented favorably to accommodate regional stresses. The imaged angle of the fault of ~30° is not shallow enough in and of itself to inhibit slip, especially given the presence of an active hydrothermal system. As described next, however, the regional strain may be influencing the ongoing slip along the Surprise Valley fault.

GPS velocity vectors indicate that the Modoc Plateau is moving away from the Basin and Range at a highly oblique, NNW-angle, at ~2 mm/year (Fig. 1) (Hammond and Thatcher, 2005). Hammond and Thatcher (2007) postulate that this motion is accommodated along the Surprise Valley fault, but the highly corrugated nature of the fault (Fig. 2) makes this unlikely. In the Eastern California Shear Zone, strain is commonly partitioned between range-front normal faults and strike-slip faults within the valley (Surpless and Miller, 2005; Wesnousky and Jones, 1994). A similar process could be at work in Surprise Valley: if dextral strike-slip motion is being accommodated within Surprise Valley, it must be occurring along a different fault system than the main SVF. Our models suggest that intra-basin faults in Surprise Valley are relatively steep (~65–70°) and that there is vertical offset of units up to hundreds of meters along them, but the lateral variations in thickness of units would make it difficult to distinguish vertical offset from lateral displacement of a unit of variable thickness. While it is likely that the majority of motion on these faults is vertical to produce the observed anomalies, it is possible that some right-lateral strike-slip motion could be accommodated along the N-trending intra-basin faults.

Given these constraints, it is possible that Surprise Valley is undergoing a transition to a new system of faults that are developing as the old one has become unfavorably oriented — either to accommodate dextral motion or to overcome frictional resistance, or a combination of the two. These transitions are difficult to resolve with geological and geophysical data, but have critical consequences for seismic hazard evaluation and geothermal prospecting. The offsets along the faults within Surprise Valley implied by the geophysical modeling suggest that these could now be accommodating the

majority of extensional strain in the region; the fact that there are so many of them may suggest that strain accommodation has not yet localized along a single fault, as would occur over time. They already appear to localize springs and hydrothermal activity, and some of their surface offset may have been overprinted by the recent presence of Lake Surprise combined with a low earthquake recurrence rate. The younger faults may also act to localize small-scale volcanic activity as indicated in our model that includes a shallow, subsurface basalt flow. While these features are well-constrained within the study area, they are less constrained to the north and south, and our ongoing work focuses on better constraining these apparently significant features.

8. Conclusions

Seismic velocity modeling confirms the presence of a shallowly east-dipping fault on the west side of Surprise Valley that puts basin fill against the bedrock of the Warner Mountains. The question remains, however, whether or not this fault is currently active.

The potential field maps and models described in this study highlight the importance of faults without significant surface expression in determining the structural setting of a basin–range system. Our data cannot be explained solely by the location of the profile in a segment boundary zone, nor by a single, shallowly-dipping normal fault bounding a basin filled with unconsolidated lake sediments. Instead, we suggest that the presence of faults within the valley may represent a transition to a new set of steeply-dipping faults to accommodate extension – possibly transtension – and uplift along this margin of the Basin and Range.

Acknowledgments

The authors thank Derek Lerch, Katie Keranen and Claudia Flores for help with velocity modeling. Joe Colgan, Simon Klemperer, and Elizabeth Miller provided very helpful conversations and reviews during the preparation of this paper. Seismic data utilized in this paper were acquired with funding from NSF grant 0444696 to Klemperer. We also thank Dave John, Gary Axen, and two anonymous reviewers for thorough and thoughtful reviews that greatly improved the organization and structure of this manuscript.

References

Anders, M.H., Schlische, R.W., 1994. Overlapping faults, intrabasin highs, and the growth of normal faults. Journal of Geology 102, 165–180.
Axen, G.J., et al., 1999. Range-front fault scarps of the Sierra El Mayor, Baja California: formed above an active low-angle normal fault? Geology 27 (3), 247–250.
Barker, B., Kennedy, M., Hoversten, M., van Soest, M.C., WIllams, K., 2005. Geothermal exploration at Fort Bidwell, California. Proceedings, Thirtieth Workshop on Geothermal Reservoir Engineering, January 31–February 2, 2005, SGP-TR-176. 5 pp.
Benoit, D., Goranson, C., Blackwell, D.D., Wesnousky, S.G., 2004. Overview of the Lake City, California geothermal system. Geothermal Resources Council Transactions 28, 311–315.
Benoit, D., Moore, J., Goranson, C., Blackwell, D.D., 2005. Core Hole Drilling and Testing at the Lake City, California geothermal field. Geothermal Resources Council Transactions 29, 203–208.
Blackwell, D.D., Leidig, M., Smith, R.P., Johnson, S.D., Wisian, K.W., 2002. Exploration and development techniques for Basin and Range geothermal systems: examples from Dixie Valley, Nevada. Geothermal Resources Council Transactions 26, 6.
Blakely, R.J., 1995. Potential theory in gravity and magnetic applications. Cambridge University Press, New York. 441 pp.
Bradshaw, G.A., Zoback, M.D., 1988. Listric normal faulting, stress refraction, and the state of stress in the Gulf Coastal Basin. Geology 16 (3), 271–274.
Brocher, T.M., 2008. Compressional and shear-wave velocity versus depth relations for common rock types in northern California. Bulletin of the Seismological Society of America 98 (2), 950–968.
Brocher, T.M., Hunter, W.C., Langenheim, V.E., 1998. Implications of seismic reflection and potential field geophysical data on the structural framework of the Yucca Mountain–Crater Flat region, Nevada. Geological Society of America Bulletin 110 (8), 947–971.
Carmichael, I.S.E., Lange, R.A., Hall, C.M., Renne, P.R., 2006. Faulted and tilted Pliocene olivine-tholeiite lavas near Alturas, NE California, and their bearing on the uplift of the Warner Range. Geological Society of America Bulletin 118 (9–10), 1196–1211.
Caskey, S.J., Wesnousky, S.G., Zhang, P., Slemmons, D.B., Louie, J.N., Abbott, R.E., 1996. Surface faulting of the 1954 Fairview Peak (MS 7.2) and Dixie Valley (MS 6.8) earthquakes, central Nevada. Bulletin of the Seismological Society of America 86 (3), 761–787.
Colgan, J.P., Egger, A.E., John, D.A., 2008a. Oligocene and Miocene arc volcanism in northeastern California. EOS Transactions AGU, Fall Meeting Supplement 89 (53), V31B–2131.
Colgan, J.P., Shuster, D.L., Reiners, P.W., 2008b. Two-phase Neogene extension in the northwestern Basin and Range recorded in a single thermochronology sample. Geology 36 (8), 631–634.
Crider, J.G., 2001. Oblique slip and the geometry of normal-fault linkage: mechanics and a case study from the Basin and Range in Oregon. Journal of Structural Geology 23 (12), 1997–2009.
Duffield, W.A., McKee, E.H., 1986. Geochronology, structure, and basin–range tectonism of the Warner Range, northeastern California. Geological Society of America Bulletin 97 (2), 142–146.
Egger, A.E., Colgan, J.P., York, C., 2009. Provenance and palaeogeographic implications of Eocene–Oligocene sedimentary rocks in the northwestern Basin and Range. International Geology Review doi:10.1080/00206810902949829.
Faulds, J.E., Varga, R.J., 1998. The role of accommodation zones and transfer zones in the regional segmentation of extended terranes. In: Faulds, J.E., Varga, R.J. (Eds.), Accommodation Zones and Transfer Zones: the Regional Segmentation of the Basin and Range Province: Geological Society of America Special Paper, vol. 323, pp. 1–45.
Fosdick, J., Egger, A.E., Colgan, J.P., Surpless, B.E., Miller, E.L., Lerch, D.W., 2005. Cenozoic evolution of the northwestern boundary of the Basin and Range; geologic constraints from the Warner Range and Surprise Valley region. Abstracts with Programs — Geological Society of America 37 (7), 70.
Friedrich, A.M., Lee, J., Wernicke, B.P., Sieh, K., 2004. Geologic context of geodetic data across a Basin and Range normal fault, Crescent Valley, Nevada. Tectonics 23 (2) 24 pp.
Glen, J.M.G., Egger, A.E., Ponce, D.A., 2008. Structural control of hot springs in a developing basin-and-range setting, Surprise Valley, California, northwestern Great Basin. Geothermal Resources Council Transactions, vol. 32. 8 pp.
Goldsworthy, M., Jackson, J., 2001. Migration of activity within normal fault systems: examples from the Quaternary of mainland Greece. Journal of Structural Geology 23, 489–506.
Griscom, A., Conradi, A., 1976. Principal facts and preliminary interpretation for gravity profiles and continuous magnetometer profiles in Surprise Valley, California. U. S. Geological Survey Open-File Report, 76-0260. 21 pp.
Hammond, W.C., Thatcher, W., 2005. Northwest Basin and Range tectonic deformation observed with the Global Positioning System, 1999–2003. Journal of Geophysical Research 110 (B10405) 12 pp.
Hammond, W.C., Thatcher, W., 2007. Crustal deformation across the Sierra Nevada, northern Walker Lane, Basin and Range transition, western United States measured with GPS, 2000–2004. Journal of Geophysical Research 112 (B05411) 26 pp.
Hedel, C.W., 1981. Map showing geothermal resources of the Lake City—Surprise Valley known geothermal resource area. Modoc County, California. U. S. Geological Survey Miscellaneous Field Studies Map, MF-1299.
Hedel, C.W., 1984. Maps showing geomorphic and geologic evidence for late Quaternary displacement along the Surprise Valley and associated faults. Modoc County, California, U. S. Geological Survey Miscellaneous Field Studies Map, MF-1299.
Jablonski, H.M., 1974. World relative gravity reference network North America. 25, U.S. Defense Mapping Agency Aerospace Center: Reference Publication 25. 1261 pp.
Kennedy, B.M., van Soest, M.C., 2006. A helium isotope perspective on the Dixie Valley, Nevada, hydrothermal system. Geothermics 35 (1), 26–43.
Kucks, R.P., Hill, P.L., Ponce, D.A., 2006. Nevada magnetic and gravity maps and data: a website for the distribution of data. U.S. Geological Survey Digital Data Series, p. 234.
Lawrence, R.D., 1976. Strike-slip faulting terminates the Basin and Range province in Oregon. Geological Society of America Bulletin 87 (6), 846–850.
Lee, J., Rubin, C.M., Calvert, A., 2001. Quaternary faulting history along the Deep Springs fault, California. Geological Society of America Bulletin 113 (7), 855–869.
Lerch, D.W., Klemperer, S.L., Stokoe, K.H., Menq, F.-Y., 2008. Integration of the NEES T-Rex vibrator and PASSCAL Texan recorders for seismic profiling of shallow and deep crustal targets. Seismological Research Letters 79 (1), 41–46.
Lerch, D.W., Klemperer, S.L., Egger, A.E., Colgan, J.P., Miller, E.L., 2010. The northwestern margin of the Basin and Range province, part 1: Reflection profiling of the moderate-angle (~30°) Surprise Valley fault. Tectonophysics 488, 142–148 (this issue).
Ludwig, W.J., Nafe, J.E., Drake, C.L., 1970. Seismic refraction. The Sea, Vol. 4, Part 1. InWiley-Intersci., New York. 53–84 pp.
Marchal, D., Guiraud, M., Rives, T., 2003. Geometric and morphologic evolution of normal fault planes and traces from 2D to 4D data. Journal of Structural Geology 25, 135–158.
Miller, E.L., Colgan, J.P., Surpless, B.E., Riedel-Bash, S., Strickland, A., Egger, A.E., Benoit, D., 2005. Drill core data from the Warner Range and Surprise Valley. Abstracts with Programs — Geological Society of America 37 (7), 203–204.
Okaya, D.A., Thompson, G.A., 1985. Geometry of Cenozoic extensional faulting: Dixie Valley, Nevada. Tectonics 4 (1), 107–125.
Oskin, M., et al., 2008. Elevated shear zone loading rate during an earthquake cluster in eastern California. Geology 36 (6), 507–510.
Pakiser, L.C., Kane, M.F., 1965. Gravity study of Owens Valley. U. S. Geological Survey Professional Paper 0470, 191–195.
Personius, S.F., Mahan, S.A., 2005. Unusually low rates of slip on the Santa Rosa Range fault zone, Northern Nevada. Bulletin of the Seismological Society of America 95 (1), 319–333.
Personius, S.F., Crone, A.J., Machette, M.N., Lidke, D.J., Mahan, Bradley, L., 2007a. Logs and scarp data from a paleoseismic investigation of the Surprise Valley fault zone, Modoc County, California. U.S. Geological Survey Scientific Investigations 2983: 2 Sheets.

Personius, S.F., Crone, A.J., Machette, M.N., Mahan, S.A., Kyung, J.B., Cisneros, H., Lidke, D.J., 2007b. Late Quaternary paleoseismology of the southern Steens fault zone, Northern Nevada. Bulletin of the Seismological Society of America 97 (5), 1662–1678.

Plouff, D., 1977. List of principal facts and gravity anomalies for an area between Orovada, Nevada, and Adel, Oregon. U.S. Geological Survey Open-File Report, OF 77-0683. 45 pp.

Ponce, D.A., 1997. Gravity data of Nevada. U.S. Geological Survey Digital Data Series, Report DDS-0042.

Ponce, D.A., Glen, J.M.G., Egger, A.E., Bouligand, C., in review. Geophysical studies in the vicinity of Warner Mountains and Surprise Valley, Northeast California, Northwest Nevada, and Southern Oregon. U.S. Geological Survey Open-File Report.

Proffett, J.M., 1977. Cenozoic geology of the Yerington District, Nevada, and implications for the nature and origin of Basin and Range faulting. Geological Society of American Bulletin 88 (2), 247–266.

Ramelli, A.R., Bell, J.W., dePolo, C.M., Yount, J.C., 1999. Large-magnitude, late Holocene earthquakes on the Genoa fault, west-central Nevada and eastern California. Bulletin of the Seismological Society of America 89 (6), 1458–1472.

Reheis, M., 1999. Extent of Pleistocene lakes in the western Great Basin. U.S. Geological Survey Miscellaneous Field Studies Map, MF-2323.

Smith, R.P., Wisian, K.W., Blackwell, D.D., 2001. Geologic and geophysical evidence for intra-basin and footwall faulting at Dixie Valley, Nevada. Geothermal Resources Council Transactions 25, 8 pp.

Snyder, D.B., Roberts, C.W., Saltus, R.W., Sikora, R.F., 1981. Magnetic tape containing the principal facts of 64,402 gravity stations in the State of California. U.S. Geological Survey Report, 2,161, PB82-168287. In: Natl. Tech. Inf. Serv. U.S. Dept. of Commer., Springfield,VA. 30 pp.

Song, J.L., ten Brink, U.S., 2004. RayGUI 2.0 — a graphical user interface for interactive forward and inversion ray-tracing. U.S. Geological Survey Open-File Report, 2004-1426.

Surpless, B.E., Miller, E.L., 2005. Strain partitioning across the central Walker Lane; geodetic and geologic constraints. Abstracts with Programs — Geological Society of America 37 (7), 203.

Surpless, B., Stockli, D.F., Dumitru, T.A., Miller, E.L., 2002. Two-phase westward encroachment of Basin and Range extension into the northern Sierra Nevada. Tectonics 21 (1) 13 pp.

Tilden, J.E., Ponce, D.A., Glen, J.M.G., Gans, K.D., 2005. Gravity and magnetic data along a seismic refraction–reflection line in northwest Nevada and northeast California. U.S. Geological Survey Open-File Report, OF 2005-1446. 12 pp.

United States Geological Survey, 1981. Total field aeromagnetic anomaly map, Surprise Valley known geothermal resource area, California. U. S. Geological Survey Open-File Report, 81-0997.

Wesnousky, S.G., Jones, C.H., 1994. Oblique slip, slip partitioning, spatial and temporal changes in the regional stress field, and the relative strength of active faults in the Basin and Range, Western United States. Geology (Boulder) 22 (11), 1031–1034.

White, D.E., 1955. Violent mud-volcano eruption of Lake City Hot Springs, northeastern California. Geological Society of America Bulletin 66, 1109–1130.

Zelt, C.A., Smith, R.B., 1992. Seismic traveltime inversion for 2-D crustal velocity structure. Geophysical Journal International 108 (1), 16–34.

Zhang, P., Mao, F., Slemmons, D.B., 1999. Rupture terminations and size of segment boundaries from historical earthquake ruptures in the Basin and Range province. Tectonophysics 308 (1–2), 37–52.